



Available online at www.sciencedirect.com



ScienceDirect

Reliability Engineering and System Safety 00 (2014) 1–27

Reliability
Engineer-
ing &
System
Safety

Coupling mode-destination accessibility with a quantitative seismic-risk assessment to identify at-risk communities

Mahalia Miller^a, Jack W. Baker^a

^aStanford University, Stanford, CA USA

Abstract

In this paper, we develop a framework for coupling mode-destination accessibility with a quantitative seismic-risk assessment to identify communities at a high risk for travel disruptions after an earthquake. For a case study of the San Francisco Bay Area, we find that accessibility varies more strongly from location to location than between income classes, and we identify particularly at-risk communities. We also observe that communities more conducive to local trips by foot or bike are predicted to be less impacted by losses in accessibility.

© 2014 Published by Elsevier Ltd.

Keywords: Infrastructure, Risk, Earthquakes

1. Introduction

Seismic risk assessment in earthquake engineering tends to focus on buildings, bridges, and the performance of infrastructure systems. For example, for measuring the performance of transportation systems, researchers typically use engineering-based metrics such as the post-earthquake connectivity loss, which quantifies the decrease in the number of origins or generators connected to a destination node [e.g., 1, 2], or the post-earthquake travel distance between two locations of interest [e.g., 3]. These frameworks have provided insight into seismic vulnerability and possible risk mitigation. However, the link to the human ramifications can be limited.

In the field of vulnerability sciences, researchers have long stressed the importance of the impact on human welfare from earthquakes. For example, Bolin and Stanford write that, “‘Natural’ disasters have more to do with the social, political, and economic aspects than they do with the environmental hazards that trigger them. Disasters occur at the interface of vulnerable people and hazardous environments” [4]. A recent World Bank and United Nations report echoed this idea that the effects on human welfare turn natural hazards into disasters [5].

Historical events emphasize the complex social effects of earthquakes. For example, on one hand the 1994 Northridge earthquake caused major damage to nine bridges, which, while significant, represented only 0.5% of the bridges estimated by Caltrans to have experienced significant shaking [6]. On the other hand, over half of businesses reported closing after the earthquake with 56% citing the “inability of employees to get to work” as a reason [7]. Furthermore, the total economic cost of transport-related interruptions (“commuting, inhibited customer access, and shipping and supply disruptions”) from this earthquake is estimated at 2.16 billion USD (2014) [8], using the consumer price index to account for inflation [9].

An emergent trend in earthquake engineering related to the social impacts is measuring the cumulative extra time needed for travel after an earthquake, sometimes called travel time delay [e.g., 10, 11]. This performance measure captures basic re-routing due to road closures and enables identifying roads more likely to be very congested. Travel

23 time approximately measures one aspect of impact on people, but does not capture the fact that some destinations
 24 and trips have higher value than others. Furthermore, this approach measures the impacts by focusing on aggregate
 25 regional effects rather than individual communities and demographic groups. Some recent work has looked at other
 26 metrics, such as the qualitative criteria-based metric “disruption index” [12]. However, this does not provide a quanti-
 27 tative link between the technical impact and the human ramifications. Other work has looked at resiliency, but defined
 28 it in pure engineering terms, such as percentage of a simplified road network that is functional [13]. Outside of trans-
 29 portation systems, some researchers have investigated the interplay between earthquake damage, such as damage to
 30 water networks, and the usability of houses and other buildings; this represents an important first step [14, 15, 16].

31 In contrast to the work on transportation-related seismic risk, urban planning has a long tradition of studying the
 32 impact on people of events and policy [17, 18]. Accessibility is one metric popular in urban planning to measure
 33 the impact of different transportation network scenarios, and it measures how easily people can get to desirable
 34 destinations [19]. This ability to travel easily is considered a measure of social impact [e.g., 20]. Furthermore,
 35 accessibility, by definition, quantifies one key aspect of human welfare [e.g., 19]. Within urban planning, accessibility
 36 has been measured in many ways, including individual accessibility, economic benefits of accessibility, and mode-
 37 destination accessibility [21]. The mode-destination accessibility is computed by taking the log value of the sum of a
 38 function of the utilities of each destination over all possible destinations and travel modes, where the utility decreases
 39 if getting to that destination is more costly or time-intensive [22]. This choice of accessibility definition is particularly
 40 applicable to quantifying the impacts of catastrophes, such as earthquakes, because certain destinations might be more
 41 critical for people in certain locations or from different socio-economic groups (such as low income or high income).

42 While recent work has investigated the interdependencies between different infrastructure networks, such as elec-
 43 tric power and water distribution [23, 24, 1], a less well-understood topic is the interdependencies within the trans-
 44 portation system itself. For example, the collapse of a highway bridge may close a transit line if the bridge crosses
 45 the transit line. Furthermore, the majority of work to date assumes that travel demand and mode choice will remain
 46 unchanged after a future earthquake, which historical data suggests is not the case [8]. A first step towards consid-
 47 ering variable demand is work in the literature that varies demand by applying a constant multiplicative factor on all
 48 pre-earthquake travel demand [10]. Thus, the prior work suggests three areas of further investigation: 1) the risk of
 49 post-earthquake accessibility losses for different people and communities in a region, 2) the impact to the risk assess-
 50 ment results of modeling interdependent transit systems, and 3) the consequences of capturing varying travel demand
 51 and different travel modes in the analysis.

52 In this paper, we develop a framework for coupling mode-destination accessibility with a quantitative seismic-risk
 53 assessment to identify at-risk populations and measure the accompanying impacts on human welfare. We illustrate
 54 our approach with a case study of the San Francisco Bay Area transportation network, including highways, local
 55 roads, and public transportation lines. We simulate earthquake scenarios, ground-motion intensity maps, and damage
 56 maps. We then compute basic network performance (travel time delay) with an efficient travel model, which includes
 57 highways and major local roads and fixed demand. Using the optimization procedure we proposed in Miller and
 58 Baker 2014 [25], we select a subset of these maps for modeling in a high-fidelity transportation model used by the
 59 local transportation authorities. Our high-fidelity model includes damage to bridges, roads, and transit lines, and
 60 varies demand using an agent-based model. While these more comprehensive models are already used in practice for
 61 general transportation planning, we extend the models to seismic risk assessment by creating an automated method for
 62 damaging and analyzing networks, in order to estimate risk in an event-based probabilistic risk framework. Finally,
 63 we analyze the predicted losses in accessibility according to 12 socio-economic groups used by local planners for the
 64 case study region, based on income class, and ratio of personal vehicles to workers in a household.

65 2. Case study: San Francisco Bay Area

66 2.1. Case study overview

67 We focus on the San Francisco Bay Area, a seismically-active region, to illustrate our approach (Figure 1). The
 68 area follows a polycentric metropolitan form, with San Francisco as the primary center and other jobs concentrated
 69 in suburban centers, such as Silicon Valley [26]. The region has a wide array of trip patterns for mandatory and
 70 non-mandatory trips. Furthermore, trip times and routes vary greatly depending on travel preferences and workplace
 71 locations [26]. Thus, we might expect noticeable disparities between households in the risk of travel time delays due
 72 to earthquakes.

73 This analysis considers the complex web of roads and transit networks of the case study area. The roads are
 74 modeled by a directed graph $G = (V, E)$, where V is a finite set of vertices representing intersections, and the set E ,
 75 whose elements are edges representing road links, is a binary relation on V . In this model, $(|V|, |E|) = (11,921, 32,858)$
 76 including centroidal links and $(|V|, |E|) = (9,635, 24,404)$ without. Centroidal links do not correspond to particular
 77 physical roads but instead capture more subtle travel flows, such as from outside the study area or the flow of people
 78 to and from some minor local roads. We also model 43 transit networks, as detailed in Miller 2014 [27].

79 We model damage to a set of 1743 highway bridges impacting the road and some transit networks, with data
 80 provided by the California Department of Transportation (Caltrans), and 1409 structures impacting the rapid transit
 81 network, BART, with data provided by that agency. We refer readers to Miller 2014 [27] for more details about
 82 matching these structures, hereafter called components, to the relevant road and transit networks.

83 2.2. Ground-motion intensity maps

84 2.2.1. Theory

85 We now describe how to produce a set of maps with ground-motion intensity realizations at each location of
 86 interest in a region and corresponding occurrence rates that reasonably capture the joint distribution of the ground-
 87 motion intensity. First, we generate Q earthquake scenarios from a seismic source model. The seismic source model
 88 specifies the rates at which earthquakes of specified magnitudes, locations, and faulting types will occur. This set of
 89 earthquake scenarios is comparable to a stochastic event catalogue in the insurance industry.

90 Second, for each earthquake scenario in the seismic source model, we use an empirical ground-motion prediction
 91 equation (GMPE) [e.g., 28, 29, 30, 31] to model Y , the resulting intensity measure at each location of interest [e.g.,
 92 32, 33, 34].

93 Then, for each of the Q earthquake scenarios, we sample b realizations of the spatially-correlated ground-motion
 94 intensity residual terms. Readers are referred to [35] for a survey of sampling methods. Once residuals are sampled,
 95 the total log ground-motion intensity (Y) is computed as

$$\ln Y_{ij} = \overline{\ln Y(M_j, R_{ij}, V_{s30,i}, \dots)} + \sigma_{ij}\epsilon_{ij} + \tau_j\eta_j \quad (1)$$

96 where j is the ground-motion intensity map index ($j = 1, \dots, m$ where $m = Q \times b$), ϵ_{ij} is the normalized within-event
 97 residual in $\ln Y$ representing location-to-location variability and η_j is the normalized between-event residual in $\ln Y$
 98 and the other parameters are defined above. Both ϵ_{ij} and η_j are normal random variables with zero mean and unit
 99 standard deviation. The vector of ϵ_{ij} can be modeled by a spatially-correlated multivariate normal distribution [e.g.,
 100 36] and the η_j by a standard univariate normal distribution.

101 The result is a set of m ground-motion intensity maps (e.g., Figure 2(a)). Since we simulate an equal number
 102 (b) of ground-motion intensity maps per earthquake scenario, the annual rate of occurrence for the j^{th} ground-motion
 103 intensity map is the original rate of occurrence of the earthquake scenario, divided by b . We denote the final result as
 104 w_j .

105 2.2.2. Implementation

106 To generate a stochastic catalog of ground-motion intensity maps, we use the OpenSHA Event Set Calculator [37].
 107 This software outputs the mean, $\overline{\ln Y_{ij}}$, and standard deviation values, σ_{ij} and τ_j , for all locations of interest for a
 108 specified seismic source model and ground-motion prediction equation. The intensity measure is the 5%-damped
 109 pseudo absolute spectral acceleration (Sa) at a period $T = 1\text{s}$, which is the required input to the fragility functions
 110 below. This spectral acceleration value represents the maximum acceleration over time that a linear oscillator with



Figure 1. Study area: San Francisco Bay Area, CA with specific travel analysis zones (TAZs) used in the case study marked in blue.

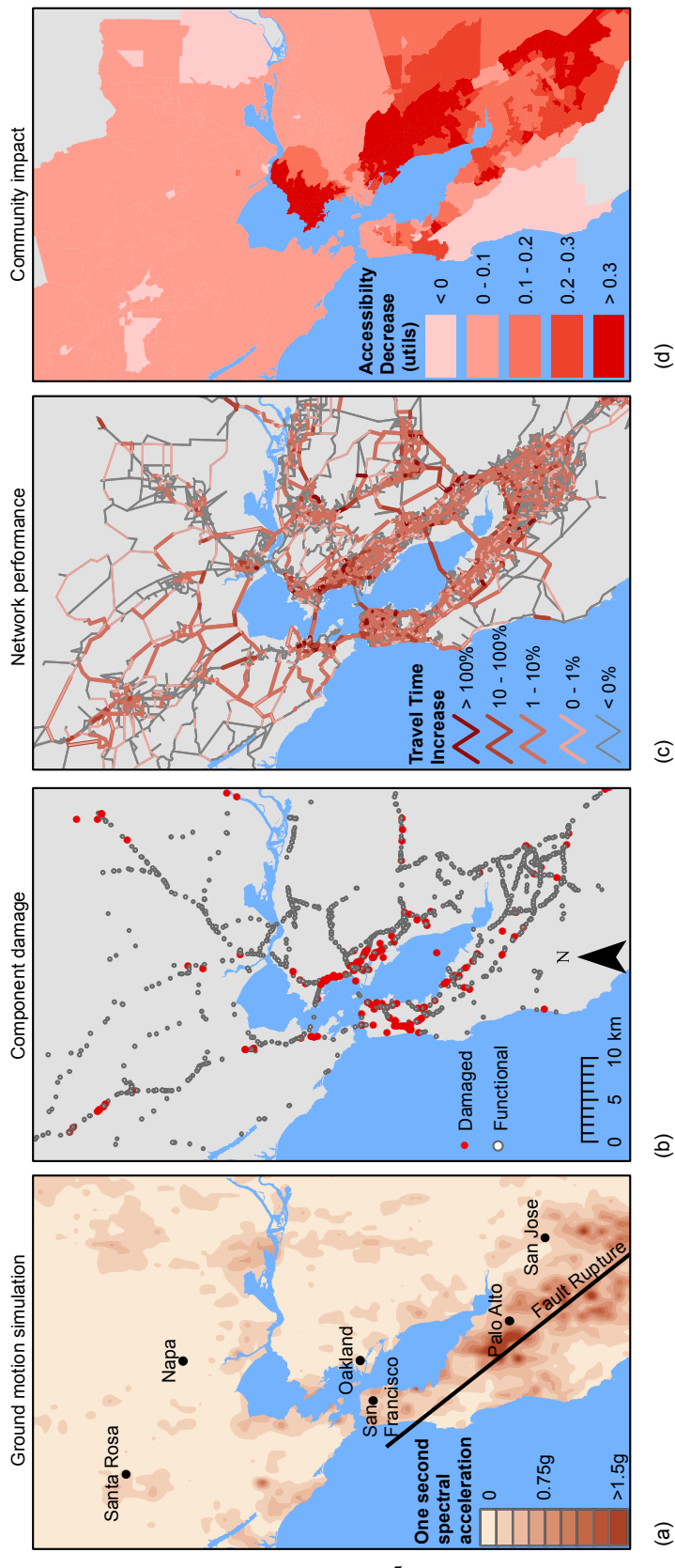


Figure 2. Illustration of the risk framework for one earthquake event including a) One-second spectral acceleration (ground-motion intensity) map with earthquake rupture, b) bridge (component) damage map, c) map of travel time increase (network-performance measure) values, and d) map of accessibility values averaged over all market segments by travel analysis zone (TAZ). There are 1454 TAZs.

111 5% damping and a period of 1 second will experience from a given ground motion. We calculate these values at
 112 each component location (bridges and other structures). Using one ground-motion intensity measure per component
 113 is a common simplification of the time-varying acceleration dynamics [e.g., 38, 11] that may have lower errors for
 114 compact components with a natural period near 1 second as opposed to long-span bridges [39]. We use the UCERF2
 115 seismic source model [40], Wald and Allen topographic slope model for the shear wave velocity $V_{s30,i}$ [41], and
 116 the Boore and Atkinson [28] ground-motion prediction equation. Using this seismic source model, which is then
 117 discretized into a list of faults and a stratified list of magnitudes and rupture locations for each, we obtain a set of 2110
 118 earthquake events on all active faults, each with an annual occurrence rate greater than or equal to 10^{-5} . We simulate
 119 the sets of maps by combining the mean terms from the Event Set Calculator and spatially-correlated residual terms
 120 of the ground-motion intensity (using [36]) according to the basic ground-motion model, Equation 1.

121 2.3. Damage maps

122 2.3.1. Theory

123 Calculating network performance risk requires assessing the structural damage of relevant components after future
 124 earthquakes. The link between ground-motion intensity and structural damage is often provided by fragility functions.
 125 Fragility functions express $P(DS_i \geq ds_S | Y_{ij} = y)$. We assume one component, such as a bridge, per site location, so we
 126 will identify both components and site locations via the index i . Using that notation, DS_i is a discrete random variable
 127 whose value represents the damage state for the i^{th} component and ds is a damage state threshold of interest. The
 128 damage state is conditioned on a realization, y , of the random variable Y_{ij} , the ground-motion intensity at the i^{th} site
 129 and j^{th} ground-motion intensity map. Researchers have calibrated fragility functions using historical post-earthquake
 130 data [e.g., 42], experimental and analytical results [e.g., 43], hybrid approaches, and expert opinion. It is possible to
 131 sample the damage states from a joint distribution that includes correlation, such as due to similarities in design or
 132 construction practices [e.g., 44, 45].

133 By sampling a damage state for each component, with probabilities obtained from the fragility functions given
 134 the ground-motion intensity, we produce a damage map (e.g., Figure 2(b)). The damage map has a realization of the
 135 damage state of each relevant component. This sampling process can be repeated multiple times to simulate multiple
 136 damage maps per ground-motion intensity map. For example, if equal numbers of damage maps are sampled per
 137 ground-motion intensity map (c damage maps per ground-motion intensity map), the weight of the j^{th} damage map
 138 should be adjusted accordingly to w_j , where $w_j = \frac{w_j}{c}$, and $j' = 1, \dots, J$.

139 *Functional percentage* relationships link the component damage to the functionality of network elements. For
 140 example, in a road network, when a bridge collapses, the traffic flow capacity of the road it carries and it crosses can
 141 be modeled as reduced to zero. These relationships are often derived from a combination of observation and expert
 142 opinion, often due to data scarcity [46]. Furthermore, the relationships are typically deterministic for a certain com-
 143 ponent damage state and restoration time [46]. Thus, in this paper, each damage map corresponds to a functionality
 144 state for every element of the network.

145 2.3.2. Implementation

146 *Component damage.* We use fragility functions of the following form to provide the link between ground-motion
 147 shaking and component damage:

$$P(DS_i \geq ds_S | Y_{ij} = y) = \Phi\left(\frac{\ln y - \lambda_{\varsigma,i}}{\xi_{\varsigma,i}}\right), \quad (2)$$

148 where Φ is the standard normal cumulative distribution function, $\lambda_{\varsigma,i}$ and $\xi_{\varsigma,i}$ are respectively the mean and standard
 149 deviation of the $\ln Y_{ij}$ value necessary to cause the ς^{th} damage state to occur or be exceeded for the i^{th} component,
 150 and the other variables are defined above. By using the previous equation and the inverse method, we can sample
 151 realizations of component damage states for a given ground-motion intensity.

152 The California Department of Transportation (Caltrans) provided the fragility function values $\lambda_{\varsigma,i}$ and $\xi_{\varsigma,i}$ used
 153 in this study for the highway components in summer 2012, which was last updated in 2007 and includes various
 154 retrofitted bridges [47]. The $\lambda_{\varsigma,i}$ values are based on component characteristics including number of spans and age
 155 as detailed in [42]. The $\xi_{\varsigma,i}$ values are given as a constant. The BART seismic safety group provided the fragility
 156 function values $\lambda_{\varsigma,i}$ and $\xi_{\varsigma,i}$ used in this study for the BART-related components for the state of the network in summer
 157 2012. At that time, data was available for the aerial structures shown in Figure ???. These correspond to the safety

158 performance goals under the recent retrofit program [48]. The numbers are comparable to the Caltrans fragility data.
 159 For the BART components, however, $\xi_{\zeta,i}$, the standard deviation of the $\ln Sa$ value necessary to cause the extensive
 160 damage state to occur or be exceeded, varies depending on the component. Both sets of fragility functions are based
 161 on the assumption that damage can be reasonably accurately estimated by the ground motion intensity at each site
 162 independently, and that the damage state can be reasonably estimated by an analytical model considering a single
 163 ground-motion intensity measure. In addition, the fragility curves do not directly consider the effects of degradation.
 164 Current work is ongoing to refine these assumptions [e.g., 49, 50, 51].

165 Caltrans also provided other component properties such as length, construction year, construction materials, out-
 166 to-out distance (the maximum distance in the perpendicular direction to traffic flow), number of spans, and average
 167 daily traffic flow). Similarly, Caltrans provided estimates for bridge replacement costs in current (2014) USD: 175 per
 168 square foot for construction and 10 per square foot for demolition of the damaged bridge [52].

169 Per ground-motion intensity map, we sample c damage maps for $c \geq 1$ (e.g., Figure 2(b)), which each has a
 170 realization of the component damage state at each component location according to the fragility function (eq. 2).
 171 The provided fragility functions do not consider correlation of the structural capacities, but other models could be
 172 used [e.g., 45].

173 *Transit network damage.* Each of the 43 transit systems we considered will be impacted differently. For Caltrain,
 174 conversations with managers suggest that given that there is one shared track system, the system would either be
 175 fully operational or not at all. Similarly, managers suggested modeling the VTA system as fully functional or not.
 176 Depending on where the BART train cars are when the earthquake strikes, the agency could accommodate different
 177 emergency plans. However, BART representatives suggested considering that if any part of a route is damaged, the
 178 entire corresponding route would not be operational (but other routes on different tracks might be still operational). In
 179 other words, each BART route as well as the Caltrain and VTA routes are each a weakest-link system, so the failure
 180 of a single component will cause the route to be non-operational. We modeled the ferry systems as fully functioning
 181 for all earthquake events. For all earthquake events including the baseline, trans-bay and cross-county bus lines were
 182 discontinued, but main lines in urban areas as well as other local bus networks were maintained per recommendations
 183 from the MTC, though they may face delays due to traffic congestion.

184 *Road network damage.* Each component damage state maps directly to the traffic capacity on associated road seg-
 185 ments. We use a functional percentage relationship to compute the traffic capacity of relevant road segments. Based
 186 on discussions with Caltrans, we consider travel conditions one week after an earthquake, since it is a critical period
 187 for decision making. For example, one week after most events, bridges should have been inspected and surface dam-
 188 age should be repaired, but major reconstruction would not have yet begun. According to our functional percentage
 189 relationship, at this point in time, the components have one of two classes of functionality, zero traffic capacity and
 190 full traffic capacity [46]. We can thus summarize the component damage using two damage states ds_s , $ds_{damaged}$ and
 191 $ds_{functional}$, which correspond to the common HAZUS *extensive* or *complete* damage states and the *none*, *slight*, or
 192 *moderate* damage states respectively [46]. Thus, the functional percentage relationship assigns zero traffic capacity
 193 on road segments that have at least one component in the $ds_{damaged}$ damage state, and full traffic capacity otherwise.
 194 We do not consider network damage from sources other than main structural damage from ground shaking, such as
 195 tunnel displacement or liquefaction, but the framework allows including such considerations. In the discussion below,
 196 we consider a set of 113,940 damage maps, which correspond to 2110 scenarios, 3 ground-motion intensity maps per
 197 scenario, and 18 damage maps per ground-motion intensity map.

198 2.4. Network performance

199 2.4.1. Theory

200 The final step for the event-based risk analysis is to evaluate the network performance measure, X . For this
 201 application, we consider a metric popular in urban planning, *mode-destination accessibility change* [e.g., 21, 53, 54,
 202 55] (e.g., Figure 2(d)). Mode-destination accessibility, hereafter referred to as accessibility, measures the distribution
 203 of travel destination opportunities weighted by the composite utility of all modes of travel to those destinations, i.e.,
 204 the ease of someone getting to different destinations weighted by how desirable those destinations are [22, 19, 56]. The

205 utility function for the mode-destination choice may be estimated using a multinomial random utility model where
 206 the logsum represents the accessibility value [57, 22, 19]. Namely, accessibility for a particular agent a is

$$Acc_a = \ln \left[\sum_{c \in C_a} \exp(V_{a(c)}) \right], \quad (3)$$

207 where $V_{a(c)}$ is the utility of the c^{th} choice for the a^{th} person for $a = 1, \dots, A$, and C_a is the choice set for the a^{th}
 208 person [22]. Choices refer to travel destinations and the mode of travel (driving, walking, bus, etc.). The units are a
 209 dimensionless quantity, *utils*. As an extension, the accessibility values from the previous equation can be converted
 210 into equivalent time and dollar amounts using *compensating variation* for cost-benefit studies; for the case study,
 211 0.0134 *utils* (generic measure of utility) equals the value of one minute per day [19, 58, 59] and we conservatively
 212 value one hour of time as approximately \$15 [60]. In other words, one *util* is worth approximately \$20 per person per
 213 day based on these assumptions. With nearly 7 million people in the region, even small changes in *utils* lead to large
 214 economic losses. Since accessibility measures how easily people can get to the destinations they desire, accessibility
 215 is used as one of the measures of human welfare [e.g., 19].

216 Furthermore, we will consider consider the fixed-demand *travel time increase* performance measure [e.g., 61, 62,
 217 11, 35]. Travel time increase is the change in the cumulative change in the amount of time every trip takes during a
 218 given time period from the pre-earthquake to post-earthquake conditions (one week post-earthquake). An example of
 219 this travel time increase for each road segment is shown in Figure 2(c).

220 2.5. Selection of event set and model description

221 We introduce two models to estimate the performance of the transportation network: a high-fidelity model and an
 222 efficient model.

223 2.5.1. Activity-based model description

224 The high-fidelity model, *Travel Model One* (version 0.3), is an activity-based model used for the official San
 225 Francisco Bay Area travel model by the Metropolitan Transportation Commission (MTC), the local metropolitan
 226 planning organization (MPO) [63]. The high-fidelity model represents the full road network as well as the public
 227 transit networks, biking, and walking. Travel demand data consists of the locations of different households in the case
 228 study area, their destination preferences and utilities, their number of vehicles, their income and other demographic
 229 data [63, 59]. More details can be found in [64]. This data was collected by the MTC from surveys and census
 230 information. Thus, we assume that the distributions of travel preferences do not change after an earthquake, although
 231 the actual destinations and trips may vary. For example, if a trip takes a very long time after a simulated earthquake,
 232 it is less likely that the trip will occur. The result is a *variable* travel demand model. This model uses a combination
 233 of Java code called CT-RAMP [65], and the Citilabs Cube Voyager and Cube Cluster software programs, which are
 234 part of a leading commercial software suite for transportation planning [66, 63]. This model differs from previous
 235 representations of this network [e.g., 67, 11, 68], since it includes not only major roads but also local roads and transit
 236 lines. We have provided further details about computing mode-destination accessibility using the high-fidelity model
 237 in Miller 2014 [27].

238 2.5.2. Efficient travel model description

239 The efficient model represents the full road network by the directed graph G and, for simplicity, does not include
 240 the transit network. The edge properties we model are flow capacity (c_f) in vehicles per hour, free-flow travel time (t_f)
 241 in minutes, congested travel time (t_a), flow (q_a) in vehicles per hour, and distance/length (d_0) in miles. The efficient
 242 model is implemented in Python using a software package intended for social network analysis, NetworkX [69],
 243 which we have leveraged for this new application. The daily travel origin-demand matrix, 2010_03_YYY, for vehicle
 244 traffic only is from the MTC and is based on travel surveys, census information, and compared with sensor data [63,
 245 70]. It is based on weekday, non-earthquake travel demand. In other words, this model assumes a fixed demand
 246 and a single transportation mode (driving), two assumptions relaxed in the high-fidelity model case above. For this
 247 efficient model, we use a version of the daily travel origin-destination matrix that is aggregated to data between all
 248 permutations of the 34 superdistricts of the San Francisco Bay Area. Superdistricts are based on population size

Income class	Income range, 1989 USD	Income range, 2014 USD
Low	0 - \$25,000	0 - \$47,334
Medium	\$25,000 - \$45,000	\$47,334 - \$85,202
High	\$45,000 - \$75,000	\$85,202 - \$142,004
Very high	more than \$75,000	more than \$142,004

Table 1. Income class definitions for the case study region, as defined by the local planning organization, the MTC [74, 59] and also translated to current 2014 USD using the consumer price index [9].

and are zones used by local authorities in a few regions, including the San Francisco Bay Area, for traffic analysis and urban planning [71]. Each superdistrict contains multiple travel analysis zones (TAZs) that represent a more granular version of superdistricts; sub-zones of the TAZs are used in the high-fidelity model. For each superdistrict, we model one centroid as a supernode, which refers to a dummy node with directed edges to a few actual nodes in the network within the target area [72]. Supernodes are advantageous for this application, because they relatively accurately capture the diffuse nature of travel demand. In contrast, if all superdistrict travel demand is inputted at one node per superdistrict with one outgoing link each, the model would be unrealistically sensitive to damage on this one link. Then, to convert from the daily travel origin-demand matrix data to hourly values, we use 5.3% of the daily travel demands, which is based on the recorded data from [73], to represent one hour of morning travel demands during the 6–10am commute period. Again, this assumes fixed travel demand. We have provided further details about computing the fixed-demand travel time using the efficient model in Miller 2014 [27].

2.5.3. Event set selection using optimization

From a large set of ground-motion intensity maps and damage maps, we choose a set of forty maps, using the optimization procedure we proposed in Miller and Baker 2014 [25]; we chose the fixed-demand travel time delay as the proxy metric, because it is related to travel time delays expected in the high-fidelity model. We then use the high-fidelity model to predict the transportation network impacts of the forty pairs of ground-motion intensity and damage maps. The outcome is forty sets of results for the target performance metric, mode-destination accessibility. Each accessibility value has a corresponding annual rate of occurrence. In the following sections, we first compare region-wide results, and then focus on particular characteristics of three communities (Figure 1 shows the study area and three communities). Finally, we discuss generalizable trends.

3. Results and Discussion

3.1. Overview of results region-wide

In this section, we analyze region-wide trends in accessibility losses for the case study area. As mentioned in Section 1, we first analyze each of the 12 socio-economic groups used in practice for the case study region [59], which are characterized based on households. The socio-economic groups correspond to all combinations of four different income classes (Table 1), and three different classes of automobile availability in the household (zero automobiles, fewer automobiles than household members that work, a greater or equal number of automobiles as compared to the number of household members that work).

We first assess the data availability for each of the segments. Each data point represents a trip by a person of a household, who is modeled as an agent in the high-fidelity transportation model. The results suggest comparing households with at least one car, because for households without cars (no cars), only the low income class has reasonably many trips (Figure 3).

General patterns emerge in the expected losses in accessibility. The expected losses are computed by taking an average of the accessibility results for each of the 1454 travel analysis zones (TAZ) for each earthquake event, weighted by the adjusted annual likelihood of occurrence from the optimization results.

First, we notice that the ratio of cars to the number of people who work in a household is correlated with accessibility risk; a higher ratio corresponds to higher expected decreases in accessibility. This corresponds to going across a column in Figure 4. For example, for the first row representing low income households, we notice a marked change in accessibility across the columns, as indicated by an expanded area of darkened TAZs from left to right (Figure 4(a-c)).

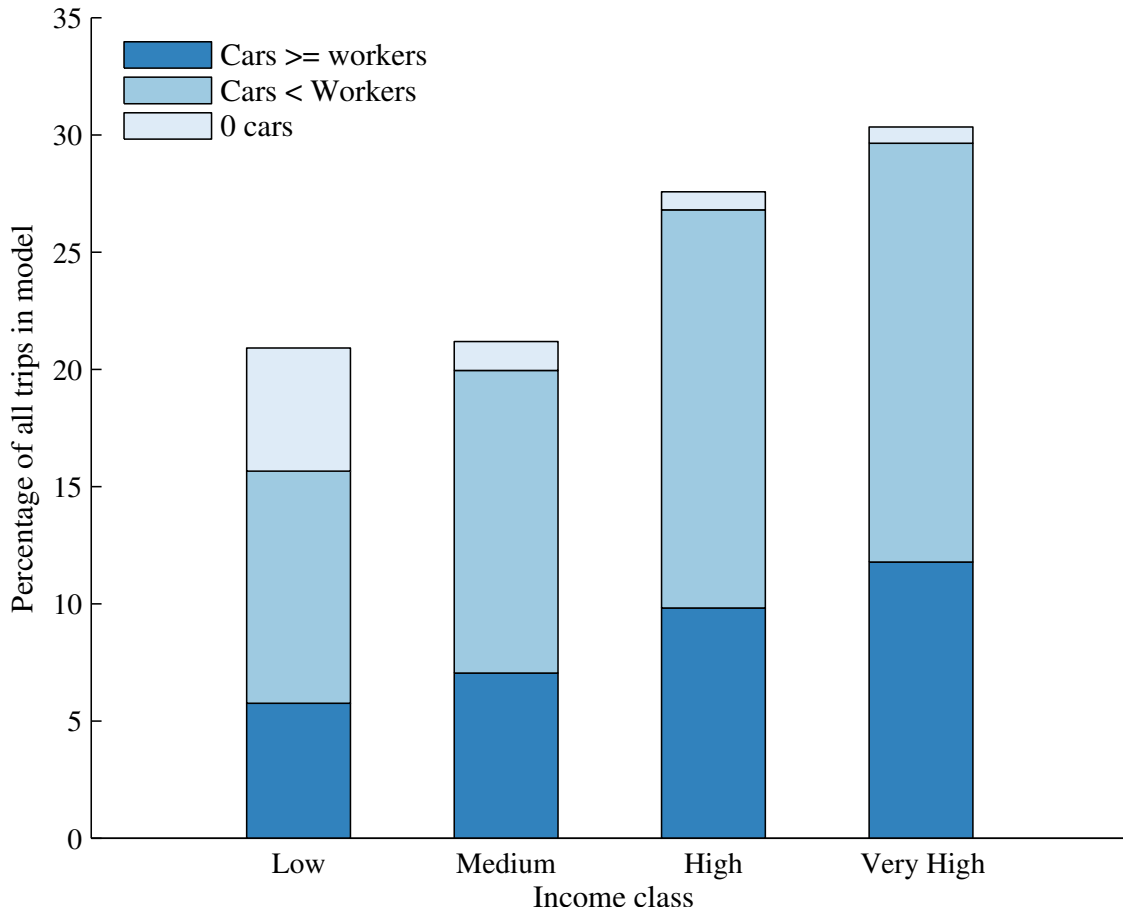


Figure 3. Percentage of total number of trips considered in the high-fidelity model by socio-economic group (determined by income class and household car ownership category) for the baseline (pre-earthquake) case.

288 Note that 1 *util* corresponds to a consumer value of compensating variation of approximately \$20 per person per day,
289 which assumes low (conservative) estimates of the value of time for travel delays and value of getting to destinations.

290 We might expect these households with more cars to take longer trips because there might be a relationship
291 between needing to travel longer distances and needing an extra car or two in a household. This is indeed the case
292 (Figure 5(b)), but it is not fully predictive. In fact, there is only a weak trend between average trip length for a TAZ
293 before any earthquake and the predicted impact on accessibility (Figure 6). Instead, we hypothesize that there are
294 other latent variables correlated with car ownership. For example, the geographic distribution of people without cars
295 varies. Additionally, in Section 3.5, we will further explore the correlation between the percentage of car-based trips
296 and accessibility risk. We will show that TAZs with fewer car-based trips, tend to have lower risk of accessibility
297 losses.

298 Second, controlling for car ownership, we see a fairly equitable distribution of risk across income class segments.
299 For example, by looking at households with fewer workers than cars (middle column of Figure 4), the variation from
300 TAZ to TAZ is significantly more striking than the difference across income segments (Figure 4(b,e,h,k)). Similarly,
301 while trip lengths are slightly longer for higher income households, the differences are subtle (Figure 5(a)).

302 Thus, for a given TAZ, the differences across incomes are not that great. At the same time though, there is
303 an unequal geographic distribution of wealth in the San Francisco Bay Area. Because of this, when we aggregate
304 accessibility risk across TAZs, we see that accessibility risk rises with increasing household income (Figure 8(b)).
305 Therefore, even though the poor are generally the most vulnerable to climatological and geophysical hazards and

306 disasters including hurricanes, floods and earthquakes [75], wealthier households in the San Francisco Bay area are
 307 more vulnerable than the other income groups to earthquake-related accessibility risk.

308 Next, we consider which geographic parts of the San Francisco Bay Area are at an elevated risk. The results show
 309 regions of high risk: in the East Bay due East of San Francisco, in the suburbs of San Jose, along the coastal and
 310 Bay-side regions South of San Francisco (Millbrae and Pacifica, e.g.), and in parts of San Francisco (South-Central
 311 neighborhoods including Westland Highlands and Glen Park neighborhoods). One may have expected more high risk
 312 areas on the San Francisco Peninsula, because of the San Andreas fault, which can generate large magnitude events.
 313 In contrast, the East Bay has higher shaking levels at more moderate return periods, due to the higher relative annual
 314 frequency of events on the Hayward Fault; this is correlated to bridge damage and thus road closures. Furthermore,
 315 the data suggests that both the more common moderate-magnitude East Bay events and the rare higher-magnitude
 316 San Andreas events can cause accessibility problems for the East Bay. Figure 7 shows one sample realization of a
 317 M6.85 Hayward event and one sample realization of a M7.45 San Andreas event—both follow the general trend of
 318 high predicted accessibility losses in the East Bay. In contrast, while any events could contribute to the risk in San
 319 Francisco, our model results show the main accessibility losses in San Francisco corresponding to the San Andreas
 320 events. Figures 7(c,d) provide one such example. Figures 7(e,f) show an example of a lower magnitude event farther
 321 away from the main population centers, a M6.35 event in the Great Valley Pittsburg-Kirby Hills Fault. This shows
 322 how the range of more minor faults in the East Bay can contribute to that area's risk. Also, we have shown the results
 323 for one socio-economic group in Figure 7, but the other socio-economic groups follow the same general patterns,
 324 albeit with different specific values.

325 Finally, we can examine the rates of loss exceedance. The annual rate, λ , of exceeding some threshold of network
 326 performance, as captured by change in accessibility, is estimated by summing the occurrence rates of all damage maps
 327 in which the performance measure exceeds the threshold:

$$\lambda_{X \geq x} = \sum_{j'=1}^J w_{j'} \mathbb{I}(X_{j'} \geq x) \quad (4)$$

328 where x is an accessibility value threshold of interest and $X_{j'}$ is the accessibility value realization for the j'^{th} damage
 329 map. The variable $w_{j'}$ is the occurrence rate of the j'^{th} damage map. The indicator function \mathbb{I} evaluates to 1 if the
 330 argument, $X_{j'} \geq x$, is true, and 0 otherwise. By evaluating λ at different threshold values, we derive an exceedance
 331 curve, Figure 8). This graph shows a similar shape to the loss exceedance curves for other performance metrics for
 332 this case study network [27]. Note that the results are primarily valid in the 100 to 2475 year return periods, since this
 333 is the range chosen for the map selection optimization problem. As a sense of scale, if we use the average value over
 334 all TAZs for this

335 Recognizing that the impact varies significantly by TAZ, as indicated by Figure 4, we also examine the accessibility
 336 loss exceedance curve for three communities: part of the San Francisco financial district, Danville, and Pacifica
 337 (Figure 1). These correspond to TAZ IDs 2, 1161, and 224 respectively. This part of the San Francisco financial
 338 district represents an area with relatively low expected changes in accessibility (Figure 4), whereas Danville and Paci-
 339 ficia are at an elevated risk in almost all socio-economic groups (Figure 4). The general trends are corroborated by
 340 the loss exceedance curves for these three communities (Figure 8(a) shows an example for the socio-economic group
 341 with medium income households with fewer cars than workers). In other words, the average middle-class person from
 342 Danville in a household with fewer cars than people who work is expected to experience travel-related losses up to 1
 343 *utils* per day after a rare earthquake, which he or she values at approximately \$20 per day considering a conservative
 344 estimate of travel time and destination value. In contrast, his or her fellow Bay Area resident in San Francisco has
 345 expected losses of only a tenth as much as experienced by a Danville resident. At return periods greater than 100
 346 years, we notice that Danville and Pacifica follow a similar general pattern, which differs dramatically from that of
 347 San Francisco.

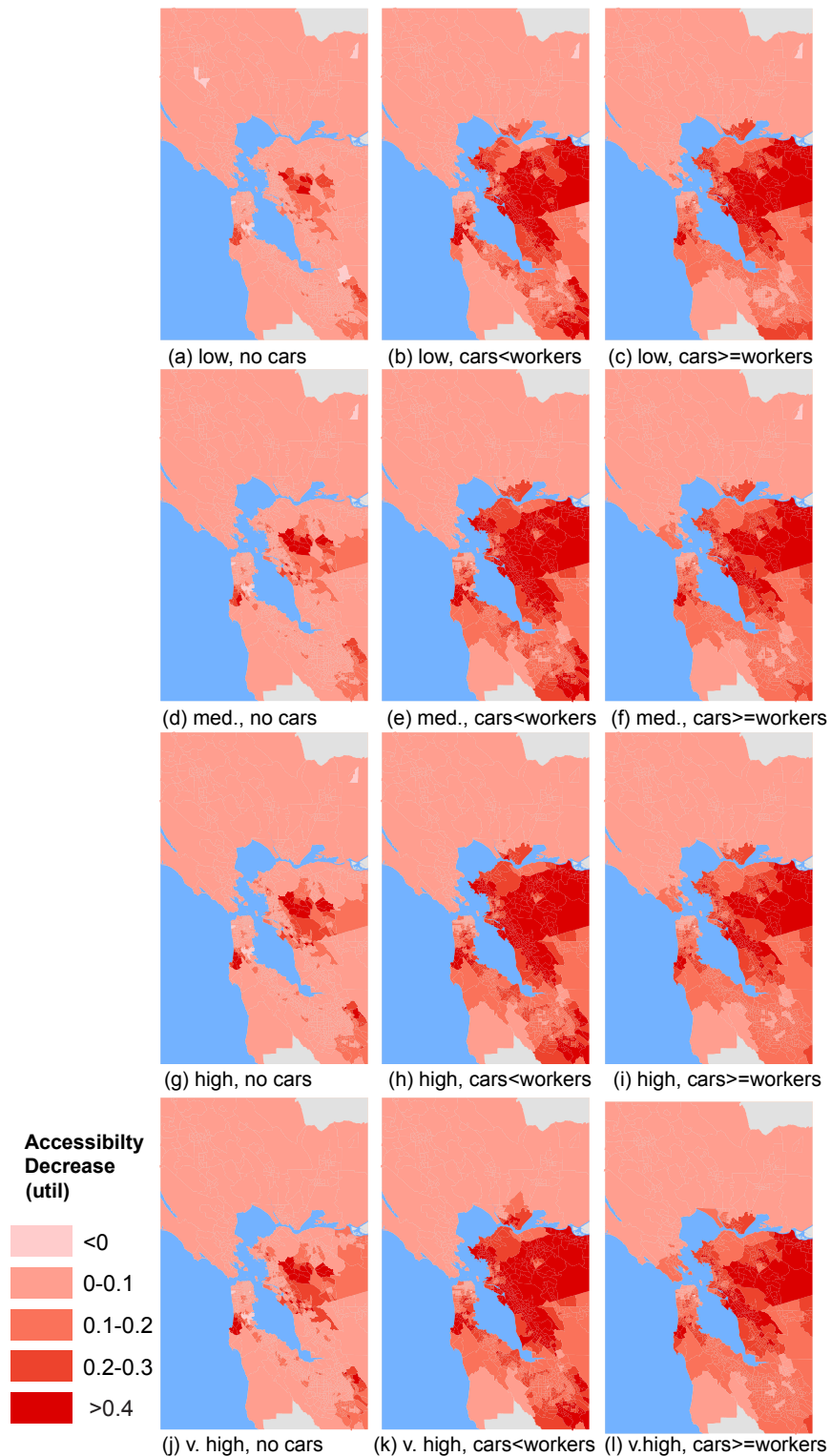


Figure 4. Expected changes in accessibility per person per day for each combination of income class and car ownership group. The darker the color, the greater the losses in accessibility.

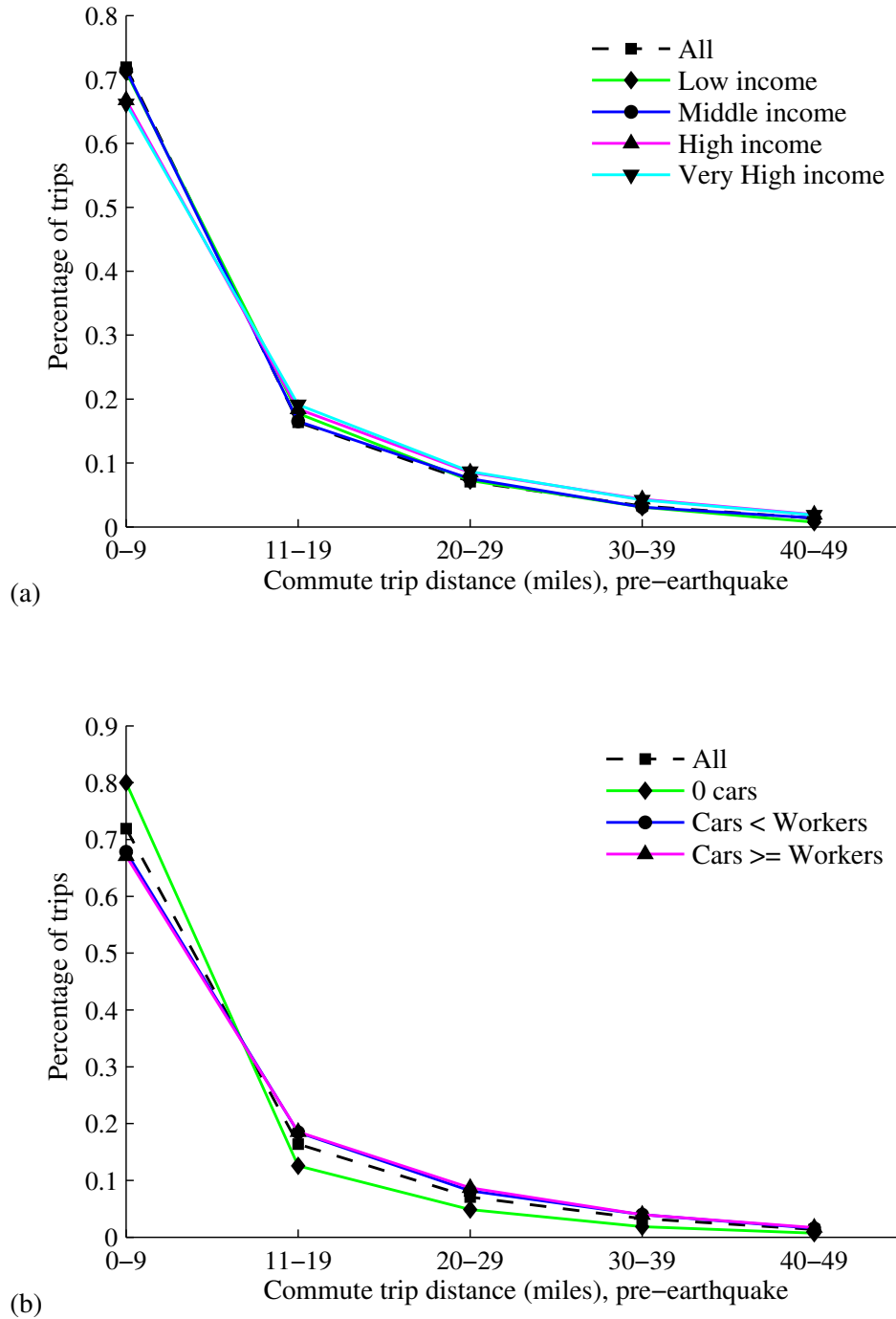


Figure 5. Distributions of commute trip length in 10-mile intervals by a) income class segment, and b) car ownership segment, (pre-earthquake)

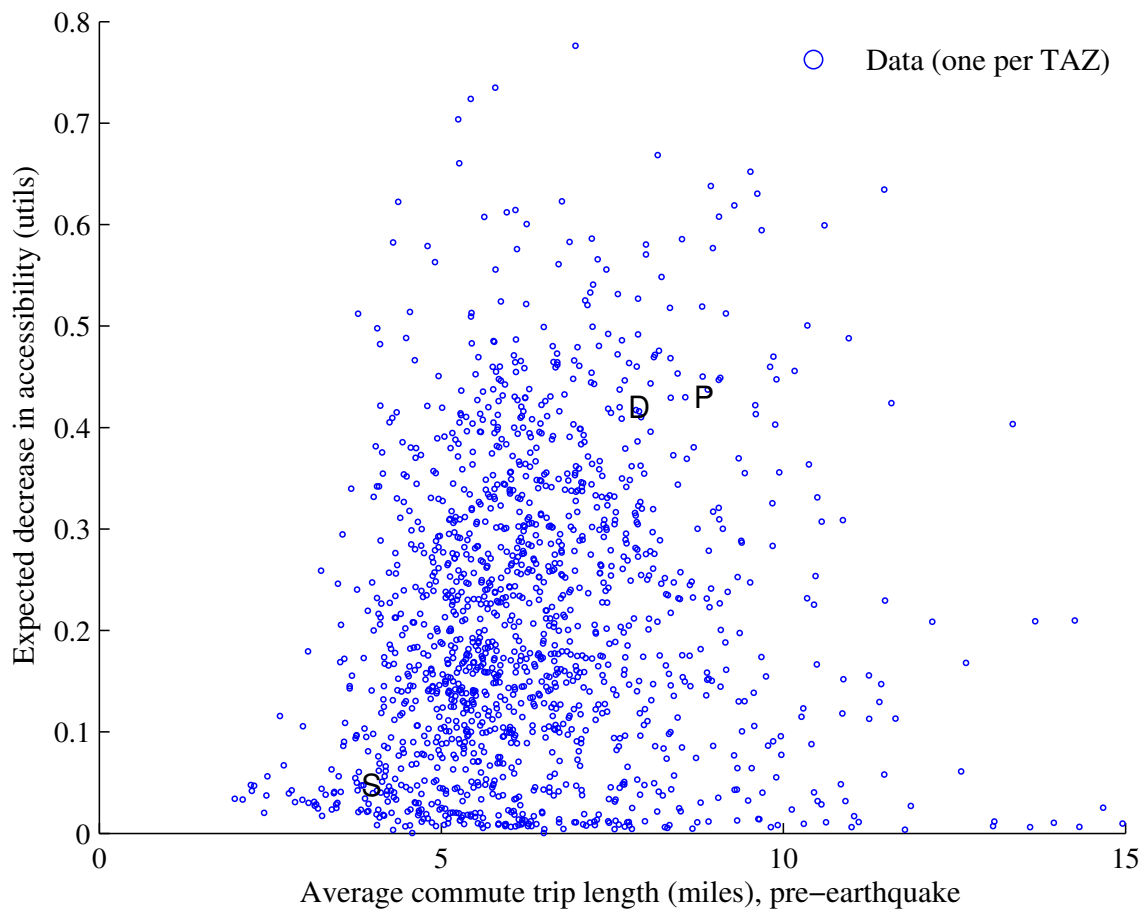


Figure 6. Trip length (pre-earthquake) versus change in total accessibility per person per day. Each dot represents one TAZ and the three case study communities, San Francisco financial district, Danville, and Pacifica are marked by S, D, and P respectively.

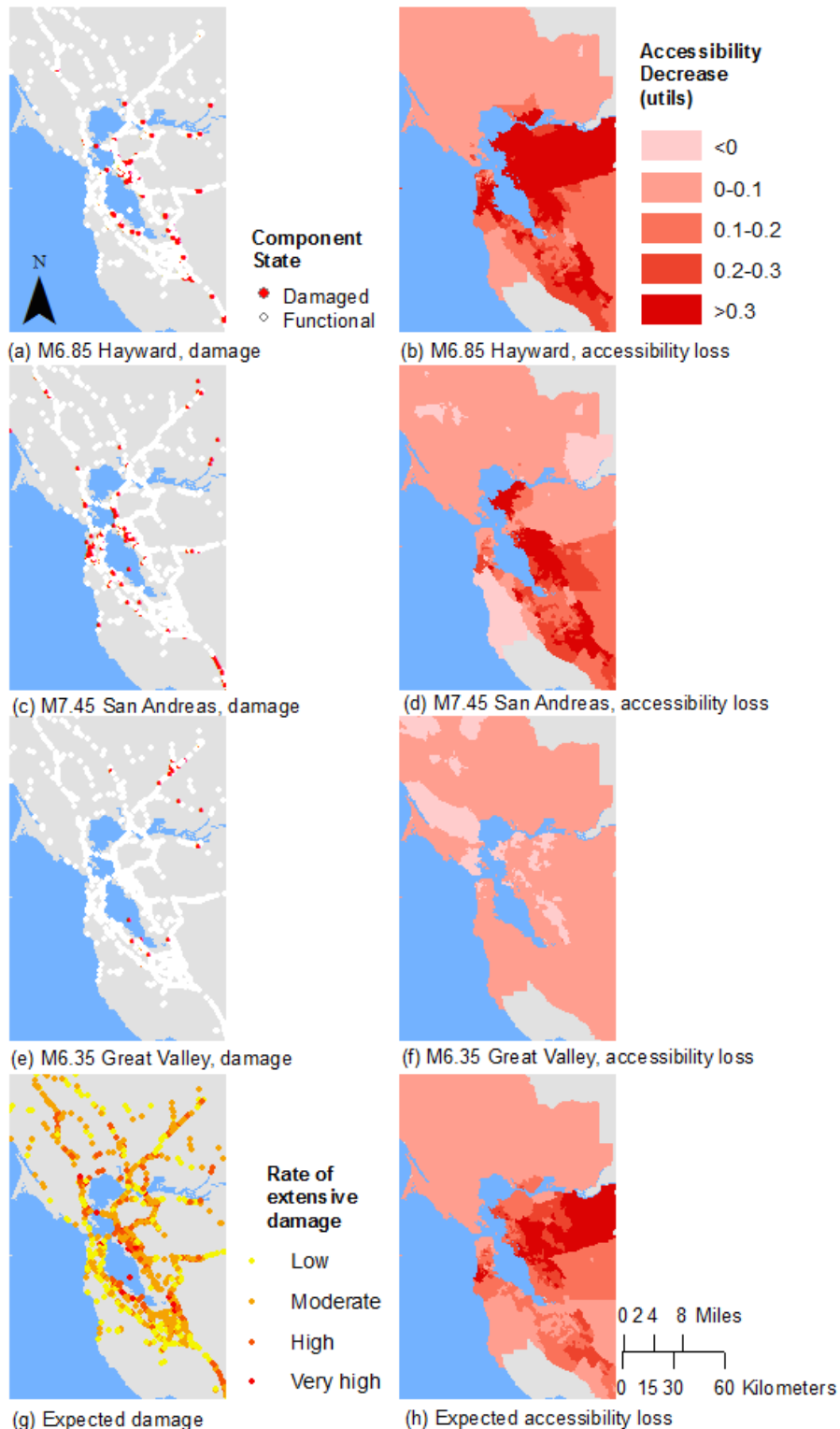


Figure 7. Bridge damage (red = damaged) and corresponding accessibility losses per person per day by TAZ for medium income households with fewer cars than workers. The bottom row has expected values calculated as a weighted average over all events.

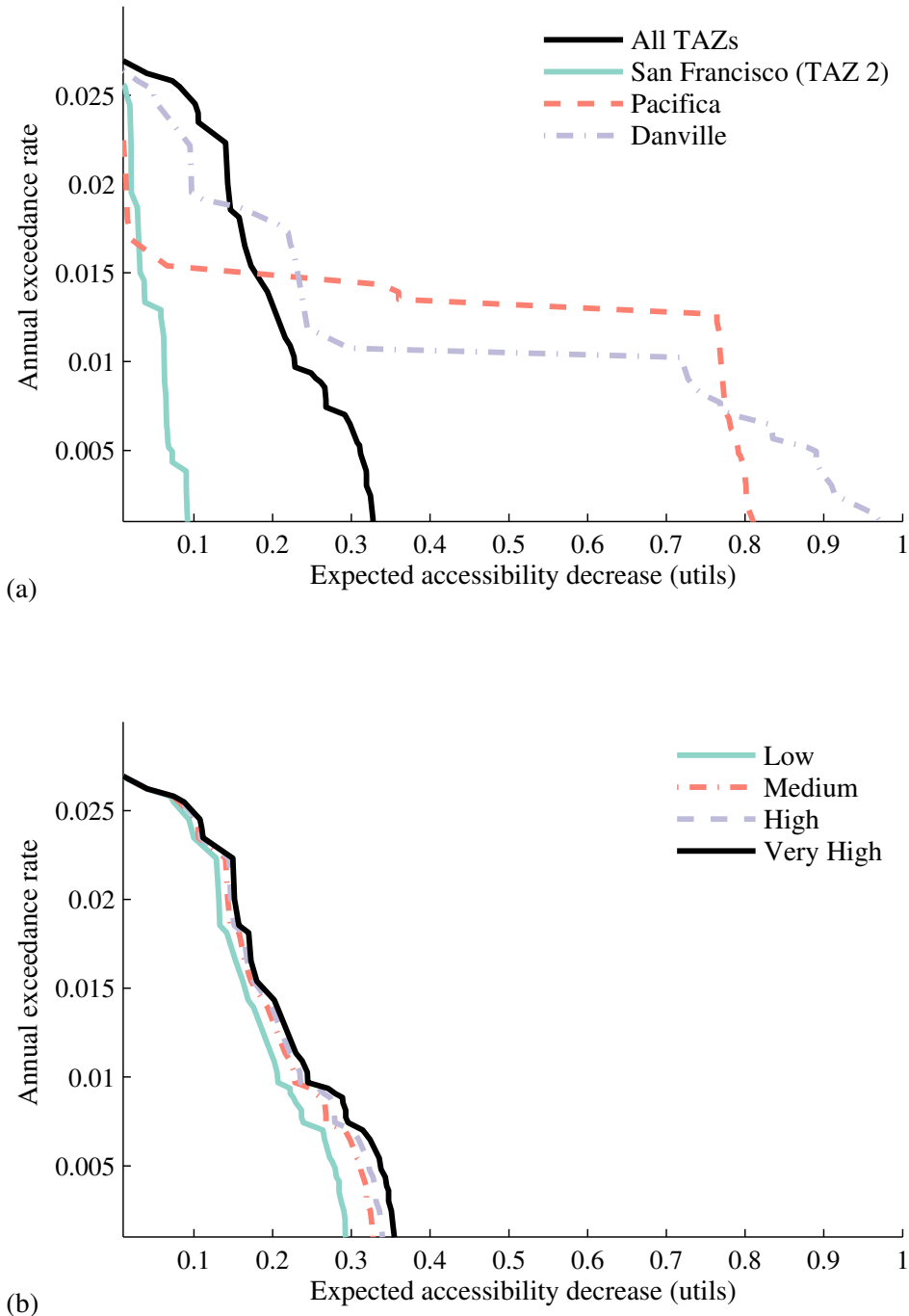


Figure 8. Accessibility annual loss exceedance curve with a comparison by (a) case study TAZs and average over all TAZs and (b) income class; all curves are in *utils* per person per day for medium income households with fewer cars than workers .

348 3.2. Analysis for San Francisco, CA financial district

349 In this section, we will explore some possible explanations for why this San Francisco TAZ (Figure 1) has lower
350 expected accessibility losses than most other communities. First, the financial district of San Francisco differs dramat-
351 ically from many other TAZs in that the percentage of trips made by car is relatively small (38% versus an average of
352 85% across all TAZs). Households traveling by foot or bike will be less influenced by network damage, because the
353 model considers only damage to the road network and transit systems; thus, foot travel routes and travel times will not
354 be affected in this model. We also observe that more trips by foot and bike correspond to destinations that are closer
355 geographically. The impact of travel mode shift post-earthquake will be further explored in Section 3.5.

356 Second, Figure 9(a) shows that the average time for a trip to and from work is about average for a TAZ in this
357 region and also follows a similar distribution to that of the other TAZs. Figure 9(b) suggests a slight trend towards
358 shorter trips, but the average trip distance for trips is only 7% lower than the average for all trips region-wide. Since
359 the trip time and length are relatively typical, but the accessibility is much lower than average, the trip time and length
360 do not explain the differences in accessibility losses.

361 In summary, the data suggests that a major cause for the low expected accessibility impact for the financial
362 district of San Francisco is the lower relative dependence on cars for mobility. In the next section, we will contrast
363 the San Francisco example with results from Pacifica, another Peninsula community that, nonetheless, is expected to
364 be at high risk of losses in accessibility.

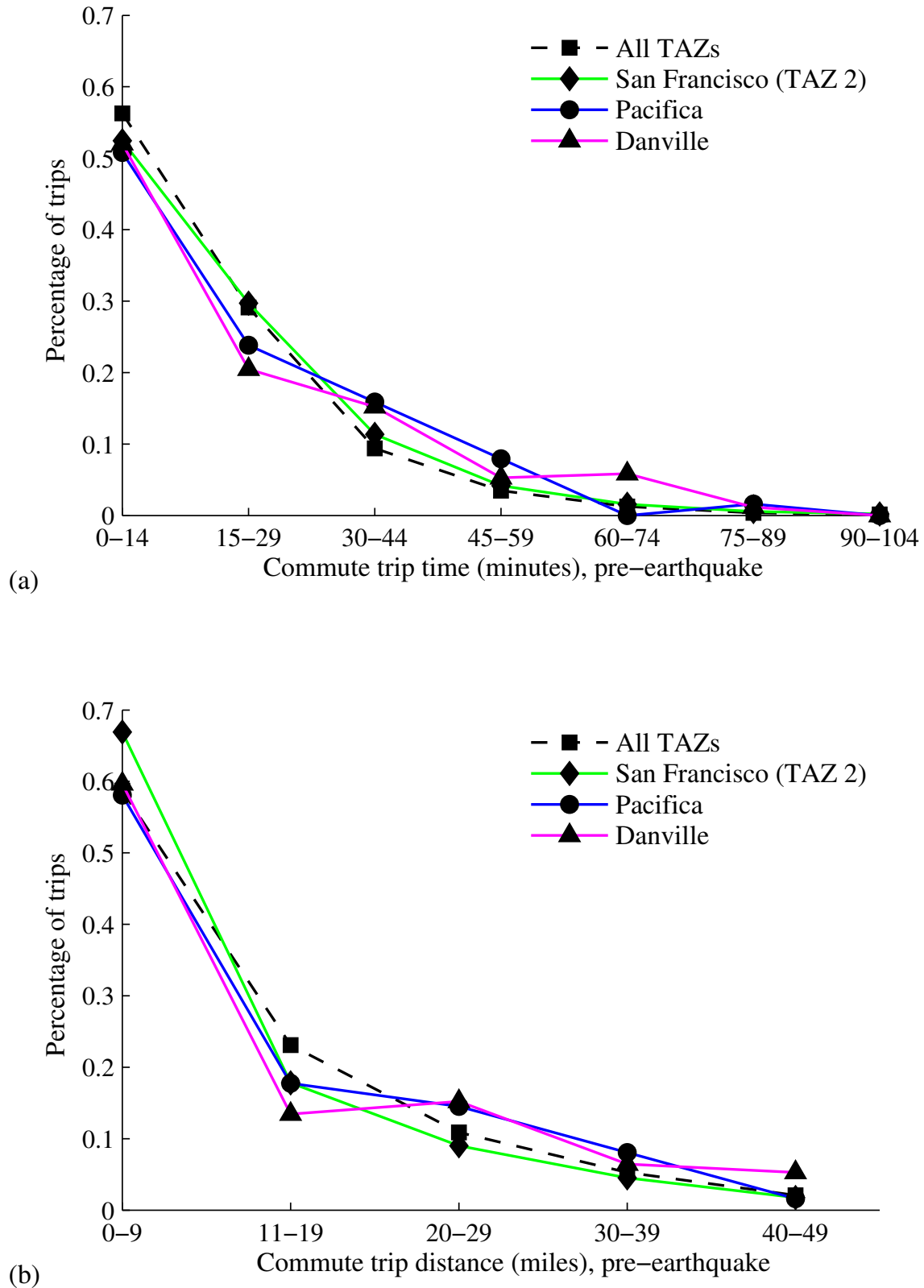


Figure 9. One-way commute trip information by (a) 15-minute time interval, and (b) 10-mile distance interval for 3 case study TAZs and the average over all TAZs.

365 3.3. Analysis for Pacifica, CA

366 We might not suspect that Pacifica, CA would be at an extremely elevated risk of accessibility losses across most
367 market segments, as compared to other communities, because it is not unusually close to a major earthquake fault.
368 In addition, the percentage of pre-earthquake car-based trips is around average for the case study area (88% versus
369 an average of 85%). In contrast to most other regions, however, Pacifica is wedged between the Pacific Ocean to
370 the West and the coastal mountains to the East. Indeed, the main access road is California Highway 1, which has
371 various vulnerable bridges included in the case study dataset. There are no viable alternative routes on local roads.
372 Since almost all trips are by car from Pacifica and the average trip length is much longer than the region-wide average
373 (108% longer), the road issue is particularly serious.

374 As a comparison, consider the next main town along the Pacific coast, Half Moon Bay, about 13 miles South.
375 Half Moon Bay has significantly lower expected accessibility losses compared to Pacifica, as illustrated in Figure 7
376 with cities labeled for reference in Figure 10. This corresponds to an expected accessibility loss of 0.43 *utils* per day
377 for a person in Pacifica in middle income household with fewer cars than workers, given an event in the dataset. In
378 comparison, a similar person in Half Moon Bay is expected only a 0.11 *utils* loss. While the seismic hazard is similar,
379 the population is about one third the size, so there is less demand for the limited road capacity [76]. Furthermore,
380 and likely most significantly, Half Moon Bay has a key alternative to California Highway 1, California Highway 92,
381 which links to Silicon Valley and the main highways of that region (US-101 and I-280). The differences in the road
382 topology are illustrated in Figure 10. Since Pacifica, CA is unusually reliant on one road with key vulnerabilities for
383 access, it has an elevated risk for losses in accessibility.

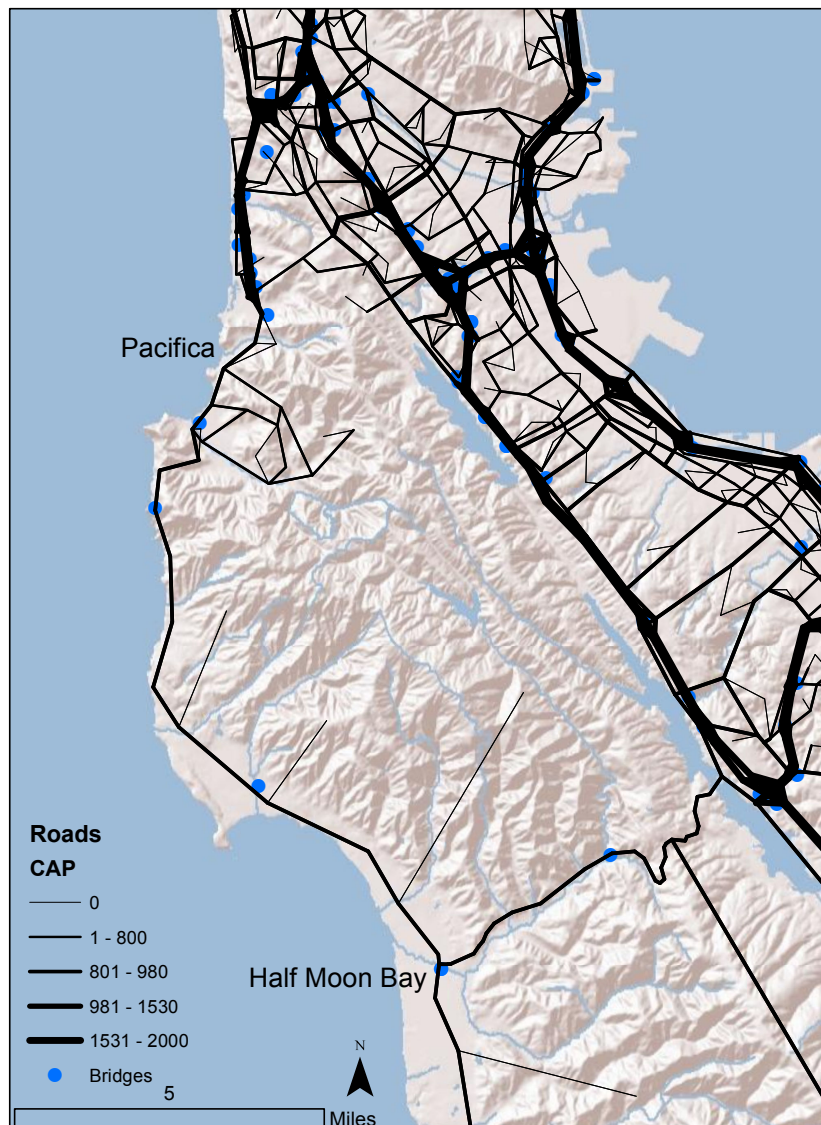


Figure 10. Differences in road access: limited roads in and out of Pacifica, CA, but an extra access highway for Half Moon Bay, CA.

384 *3.4. Analysis for Danville, CA*

385 We will first examine the trip length characteristics for Danville, CA. As illustrated in Figure 9, the distribution
 386 of pre-earthquake commute trips from Danville, CA is shifted towards both longer distance and longer time than the
 387 communities we have studied so far with a relatively higher proportion of trips taking 60–74 minutes and traveling
 388 over 40 miles than in the other communities. The same trend holds for other trip purposes. On average, the trip lengths
 389 are longer than many other TAZs (85% longer than the average over all trips originating from any of the TAZs). The
 390 consequence of these longer trips is more opportunities to be impacted by a road closure, simply because more roads
 391 and bridges will be used. Moreover, the road layout near Danville, CA mandates many highway trips, which increase
 392 the likelihood of crossing bridges; bridges are the part of the network for which we model the vulnerability.

393 Next, we look at patterns of expected bridge damage. Bridge damage is important for many regions, including
 394 Danville, because the percentage of car-based trips is high (85% of all trips on average, and also 85% of Danville-
 395 origin trips). For damage map realizations for the three earthquake events we introduced—M6.85 Hayward Fault,
 396 M7.45 San Andreas Fault, M6.35 Great Valley Fault—some bridges in the Oakland area are in the extensive or
 397 greater damage state (Figure 7(a,c,e)). These correspond to bridge closures in the model. In addition, in the first two
 398 cases, there are closures to the north of Danville, which represents one of the two main travel routes from Danville.
 399 There are also scattered closed bridges to the west of Danville, likely a top travel corridor because of the workplace
 400 centers in San Francisco, Oakland, and Silicon Valley (all to the west). As for transit, in the first two events, all BART
 401 lines are closed, so there are limited alternatives to the popular road routes. The result is that the residents of Danville,
 402 CA have reduced access to their normal destinations after all these events.

403 We can also look at bridge damage in a probabilistic event-set-based manner. The expected damage over all
 404 events represents the annual rate of a bridge being in the extensive or complete damage state for the set of 113,940
 405 damage maps (Figure 7(g)). This figure indicates that bridges in the Oakland–Berkeley area are particularly likely to
 406 be damaged. We also see a few high likelihood bridges to the North of Danville. Thus, the data suggests that the
 407 relative position of high-risk bridges to Danville contributes to this community’s accessibility risk.

408 3.5. Impact of travel mode shifts and regional variations in travel mode patterns

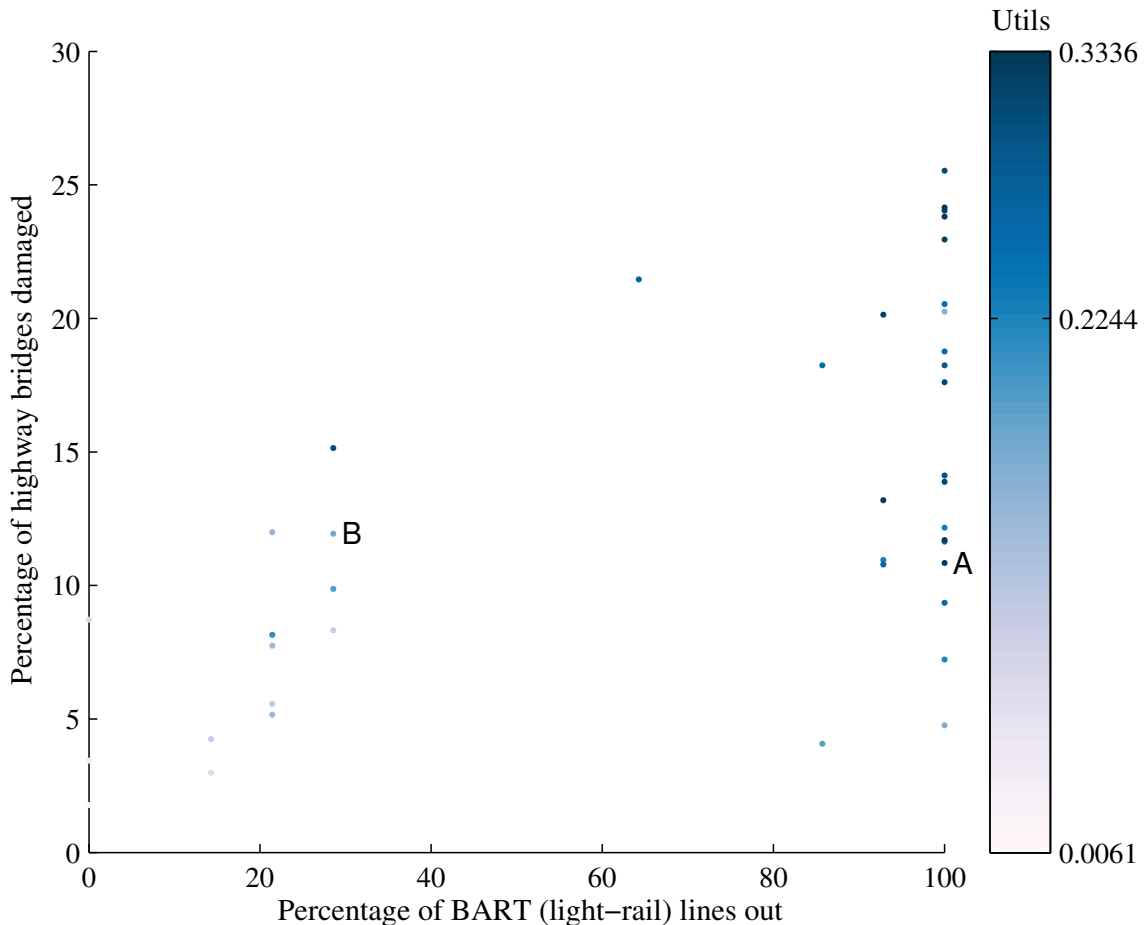


Figure 11. Percentage of BART (heavy-rail) lines not operational versus percentage of highway bridges damaged, where each data point corresponds to one earthquake damage map. The values are color-coded by the average loss in accessibility per day per person over all TAZs for households with the fewer cars than people who work. Two events discussed in this section are marked by the letters A and B.

409 First, we compare patterns of transit system damage with patterns of travel mode shifts after earthquake events.
 410 Over all the simulated events, taking a weighted average by the annual likelihood of each event, we see a reduction in
 411 transit ridership (25% weighted average decrease from the base case). This is not surprising. The heavy rail systems
 412 (BART and Caltrain) are not fully operational in most of the forty simulated events (Table 2), and these have heavy
 413 ridership. The light rail systems (VTA and Muni light rail) also suffered losses in many events (Table 2). As detailed
 414 in Miller 2014 [27], with regards to the other transit systems, trans-bay and cross-county bus lines were suspended
 415 in the forty events and the baseline case; main local buses are modeled as operational, although with possible delays;
 416 and ferries are modeled as operational. The result is an average increase in the percentage of trips by the other modes
 417 (foot, car, and bike).

418 A notable exception is the M6.35 Great Valley, Pittsburg-Kirby Hills Fault earthquake event, as illustrated in
 419 Figure 7(e,f). In this event, there were no line closures on the major transit systems (BART, Caltrain, Muni, and
 420 VTA Light Rail). There were, however, some bridge closures on the highways (Figure 7(e)). The result was a slight
 421 increase in transit ridership and also in trips by foot.

422 In general, accessibility impact grows with increasing number of damaged transit lines, particularly in combination
 423 with high numbers of damaged bridges (Figure 11). The results do not conclusively show that transit is a key
 424 contributor to accessibility risk, but based on individual examples, the data suggests this conclusion. For example,

Functionality	BART	Caltrain	Muni Light Rail	VTA Light Rail
Full	3	13	25	9
50-99%	10	0	15	0
1-49%	8	0	0	0
None	19	27	0	31

Table 2. Transit network functionality as a count out of the forty simulated events for BART, Caltrain, Muni Light Rail, and VTA Light Rail. Functionality is measured by the percentage of lines that are operational given a damage map (based on a ground-motion intensity map).

in the set of forty events analyzed with the high-fidelity model, the M6.85 Hayward Rogers-Creek and the M7.45 Northern San Andreas Fault event both have a similar number of damaged bridges (around 11%); these are noted by points A and B respectively in Figure 11. These correspond to the bridge damage and accessibility maps in Figures 7(a,b) and 7(c,d) respectively. However, this Hayward Rogers-Creek event has significantly higher accessibility impact. Similarly, the transit impact was different. This Northern San Andreas event had only 4 of the 14 BART lines, all Caltrain, and all VTA Light Rail lines not operational, whereas this Hayward Rogers-Creek event had all 14 of the 14 BART lines, all Caltrain, all VTA Light Rail and 3 of the 8 Muni light rail lines not operational. Thus, the transit lines were impacted significantly differently. Moreover, the differences in accessibility results could not have been predicted from the efficient transportation model, because the percent of damaged bridges was about the same, and the San Andreas event actually corresponded to a greater increase in travel time.

Second, we examine the correlation between a community's walkability, as measured by the percentage of total trips made by that travel mode, and the expected decrease in accessibility by community. We see that an increased percentage of pre-earthquake trips on foot corresponds to a lower average decrease in accessibility (Figure 12). This result corroborates the specific example of the San Francisco Financial District we saw in Section 3.2. Furthermore, on average, the number of by-foot trips slightly increases after the earthquake events where road congestion worsens. This model result is consistent with the observations after the 1995 Kobe earthquake, in which many commuters switched to walking and biking ("non-mechanized modes") in the weeks after the earthquake [8]. In conclusion, the data suggests that TAZs, i.e. communities, which have a greater walkability are also more resilient to earthquake-related accessibility risk.

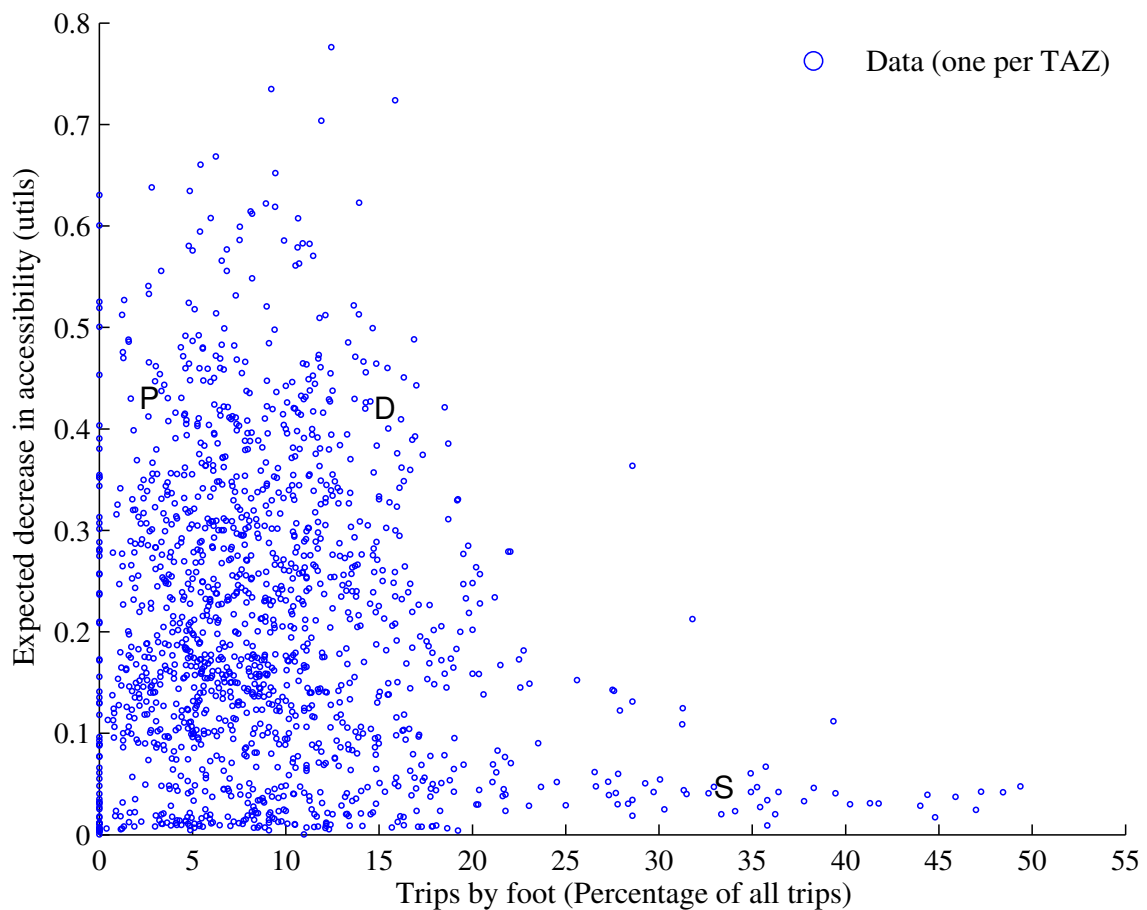


Figure 12. Percentage of total trips by foot (pre-earthquake) versus decrease in total accessibility, measured in *utils* per day (for households with the number of cars less than the number of workers). Each dot represents one TAZ and the three case study communities, San Francisco financial district, Danville, and Pacifica are marked by S, D, and P respectively.

444 **4. Conclusions**

445 Here we have shown how mode-destination accessibility links post-earthquake infrastructure damage to the impact
 446 on human welfare and enables identifying at-risk geographic and demographic groups in a region. Adopting this
 447 performance metric from the urban planning community, we have illustrated its use for seismic risk assessment and
 448 mitigation through a case study of the San Francisco Bay Area. Furthermore, we have proposed a model that captures
 449 transport mode choice and the interdependencies of the roads and transit systems. We have nested this network
 450 performance model within an event-based probabilistic seismic risk framework. In the case study, we first simulated
 451 a large set of earthquake scenarios, ground-motion intensity maps, and damage maps. Then, we used optimization
 452 to select a subset of the maps. After that, for each of the selected maps, we processed the data for analysis in a
 453 high-fidelity, activity-based travel model that includes the road network, transit networks, walking and biking options,
 454 variable travel demand, and mode choice. From this, we computed the mode-destination accessibility, a state-of-
 455 the-art performance measure for each community and each socio-economic group (defined by income class and car
 456 ownership).

457 We saw stark differences in accessibility from location to location. Specifically, we found that areas in the suburbs,
 458 such as the far East Bay, South San Jose and select communities just south of San Francisco, were particularly at risk.
 459 We found that these geographic trends persisted across income classes and car ownership groups. Nonetheless, on
 460 average, higher income households with more cars than workers had the highest risk across the studied socio-economic
 461 groups. One key reason is the geographic clustering of these households in higher-risk areas. Another factor is that
 462 these households tend to take longer daily trips, thus crossing more roads and bridges and possibly increasing the
 463 likelihood of disruption.

464 The third finding from this study is that travel modes shift after an earthquake, and communities who can more
 465 easily make these adjustments are generally predicted to experience lower post-earthquake losses in accessibility. The
 466 results suggest that the walkability of a community, as measured by the percentage of pre-earthquake trips by foot, is
 467 closely linked to reduced accessibility risk. We also found that one adaptation measure after major earthquakes is an
 468 increased likelihood to walk or bike. We also found that in almost all of the simulated earthquake events, the transit
 469 system, particularly the heavy rail (BART and Caltrain) lines, is predicted by this model to be severely impacted. The
 470 result is a reduced mode share for transit and increased trips by the other modes (car, walk, bike). Thus, this study
 471 suggests that not including transit can lead to an unconservative estimate of seismic risk of transportation systems. The
 472 model shows, however, that when transit is not damaged—which is very rare for this case study—ridership increases.

473 In conclusion, mode-destination accessibility offers important applications for further investigation into the impact
 474 to human welfare of engineering losses and mitigation efforts. In addition, we have provided researchers a method
 475 for including the interdependencies of the transportation system into an event-based probabilistic risk framework.
 476 This work lays the foundation for future work in risk mitigation and policy to reduce the vulnerability of at-risk
 477 communities. It also suggests that initiatives making communities more conducive for cycling and walking to work
 478 can increase resiliency.

479 **References**

- 480 [1] L. Dueñas-Osorio, J. I. Craig, B. J. Goodno, Seismic response of critical interdependent networks, *Earthquake Engineering & Structural*
 481 *Dynamics* 36 (2) (2007) 285306. doi:10.1002/eqe.626.
- 482 [2] Y.-J. Lee, J. Song, P. Gardoni, H.-W. Lim, Post-hazard flow capacity of bridge transportation network considering structural deterioration of
 483 bridges, *Structure and Infrastructure Engineering* 7 (7-8) (2011) 509521. doi:10.1080/15732479.2010.493338.
- 484 [3] S. E. Chang, M. Shinohzuka, J. E. Moore, Probabilistic earthquake scenarios: Extending risk analysis methodologies to spatially distributed
 485 systems, *Earthquake Spectra* 16 (3) (2000) 557–572. doi:10.1193/1.1586127.
- 486 [4] R. C. Bolin, L. Stanford, *The Northridge earthquake: vulnerability and disaster*, Routledge, London; New York, 1998.
- 487 [5] The World Bank and the United Nations, *Natural hazards, unnatural disasters: the economics of effective prevention*, Tech. rep., The World
 488 Bank, Washington D.C. (2010).
- 489 [6] California. Dept. of Transportation. Post Earthquake Investigation Team, *Northridge earthquake, 17 January 1994: PEQIT report*, California
 490 Department of Transportation, Division of Structures, Sacramento, 1994.
- 491 [7] K. J. Tierney, Business Impacts of the Northridge Earthquake, *Journal of Contingencies and Crisis Management* 5 (2) (1997) 87–97.
 492 doi:10.1111/1468-5973.00040.
- 493 [8] P. Gordon, H. W. Richardson, B. Davis, Transport-related impacts of the Northridge earthquake, *National Emergency Training Center*, 1998.
- 494 [9] United States Department of Labor, *Guide to available CPI data* (2014).

- [10] A. Kiremidjian, J. Moore, Y. Y. Fan, O. Yazlali, N. Basöz, M. Williams, Seismic risk assessment of transportation network systems, *Journal of Earthquake Engineering* 11 (3) (2007) 371–382. doi:10.1080/13632460701285277.
- [11] N. Jayaram, J. W. Baker, Efficient sampling and data reduction techniques for probabilistic seismic lifeline risk assessment, *Earthquake Engineering & Structural Dynamics* 39 (10) (2010) 1109–1131. doi:10.1002/eqe.988.
- [12] C. S. Oliveira, M. A. Ferreira, F. M. d. S., The concept of a disruption index: application to the overall impact of the july 9, 1998 faial earthquake (azores islands), *Bulletin of Earthquake Engineering* 10 (1) (2012) 7–25. doi:10.1007/s10518-011-9333-8.
- [13] P. Bocchini, D. M. Frangopol, Restoration of bridge networks after an earthquake: Multicriteria intervention optimization, *Earthquake Spectra* 28 (2) (2012) 426–455. doi:10.1193/1.4000019.
- [14] F. Cavalieri, P. Franchin, P. Gehl, B. Khazai, Quantitative assessment of social losses based on physical damage and interaction with infrastructural systems, *Earthquake Engineering & Structural Dynamics* 41 (11) (2012) 1569–1589. doi:10.1002/eqe.2220.
- [15] B. Khazai, B. Vangelsten, S. Duzgun, J. Braun, J. Daniell, Social impacts of emergency shelter provision in the aftermath of earthquakes: Integrating social vulnerability in systemic seismic vulnerability analysis, in: *Geophysical Research Abstracts*, Vol. 13, 2011, pp. 7374–7374.
- [16] C. G. Burton, *Social vulnerability* (2014).
URL <http://www.globalquakemodel.org/what/physical-integrated-risk/socio-economic-vulnerability/>
- [17] R. Unwin, *Town planning in practice: An introduction to the art of designing cities and suburbs*, T. Fisher Unwin, 1909.
- [18] F. S. Chapin, *Urban land use planning*, University of Illinois Press, 1970.
- [19] D. A. Niemeier, Accessibility: an evaluation using consumer welfare, *Transportation* 24 (4) (1997) 377396.
- [20] C. A. Kennedy, A comparison of the sustainability of public and private transportation systems: Study of the greater toronto area, *Transportation* 29 (4) (2002) 459–493. doi:10.1023/A:1016302913909.
- [21] K. T. Geurs, B. van Wee, Accessibility evaluation of land-use and transport strategies: review and research directions, *Journal of Transport Geography* 12 (2) (2004) 127–140. doi:10.1016/j.jtrangeo.2003.10.005.
- [22] S. L. Handy, D. A. Niemeier, Measuring accessibility: an exploration of issues and alternatives, *Environment and Planning A* 29 (7) (1997) 11751194.
- [23] I. Hernandez-Fajardo, L. Dueñas-Osorio, Probabilistic study of cascading failures in complex interdependent lifeline systems, *Reliability Engineering & System Safety* 111 (2013) 260–272. doi:10.1016/j.ress.2012.10.012.
- [24] I. Hernandez-Fajardo, L. Dueñas-Osorio, Sequential propagation of seismic fragility across interdependent lifeline systems, *Earthquake Spectra* 27 (1) (2011) 23–43. doi:10.1193/1.3544052.
- [25] M. Miller, J. Baker, Ground-motion intensity and damage map selection for probabilistic infrastructure network risk assessment using optimization, in review (2014).
- [26] R. Cervero, K.-L. Wu, Polycentrism, commuting, and residential location in the San Francisco Bay area, *Environment and Planning A* 29 (5) (1997) 865–886.
- [27] M. Miller, *Seismic risk assessment of complex transportation networks*, PhD thesis, Stanford University (2014).
- [28] D. M. Boore, G. M. Atkinson, Ground-motion prediction equations for the average horizontal component of PGA, PGV, and 5%-damped PSA at spectral periods between 0.01 s and 10.0 s, *Earthquake Spectra* 24 (1) (2008) 99–138.
- [29] N. Abrahamson, W. Silva, Summary of the Abrahamson & Silva NGA Ground-Motion Relations, *Earthquake Spectra* 24 (1) (2008) 67–97. doi:10.1193/1.2924360.
- [30] B. Chiou, R. R. Youngs, An NGA model for the average horizontal component of peak ground motion and response spectra, *Earthquake Spectra* 24 (1) (2008) 173–215. doi:10.1193/1.2894832.
- [31] K. W. Campbell, Y. Bozorgnia, NGA ground motion model for the geometric mean horizontal component of PGA, PGV, PGD and 5% damped linear elastic response spectra for periods ranging from 0.01 to 10s, *Earthquake Spectra* 24 (1) (2008) 139–171. doi:10.1193/1.2857546.
- [32] K. W. Campbell, Strong motion attenuation relations: A ten-year perspective, *Earthquake Spectra* 1 (4) (1985) 759–804. doi:10.1193/1.1585292.
- [33] J. W. Baker, C. A. Cornell, Which spectral acceleration are you using?, *Earthquake Spectra* 22 (2) (2006) 293–312. doi:10.1193/1.2191540.
- [34] R. Foulser-Piggott, P. J. Stafford, A predictive model for Arias intensity at multiple sites and consideration of spatial correlations, *Earthquake Engineering & Structural Dynamics* 41 (3) (2012) 431451. doi:10.1002/eqe.1137.
- [35] Y. Han, R. A. Davidson, Probabilistic seismic hazard analysis for spatially distributed infrastructure, *Earthquake Engineering & Structural Dynamics* 41 (15) (2012) 2141–2158. doi:10.1002/eqe.2179.
- [36] N. Jayaram, J. W. Baker, Correlation model for spatially distributed ground-motion intensities, *Earthquake Engineering & Structural Dynamics* 38 (15) (2009) 1687–1708. doi:10.1002/eqe.922.
- [37] E. H. Field, T. H. Jordan, C. A. Cornell, OpenSHA: a developing community-modeling environment for seismic hazard analysis, *Seismological Research Letters* 74 (4) (2003) 406 – 419. doi:10.1785/gssrl.74.4.406.
- [38] M. Shinozuka, Y. Murachi, X. Dong, Y. Zhou, M. J. Orlikowski, Effect of seismic retrofit of bridges on transportation networks, *Earthquake Engineering and Engineering Vibration* 2 (2) (2003) 169–179. doi:10.1007/s11803-003-0001-0.
- [39] K. Konakli, A. Der Kiureghian, Simulation of spatially varying ground motions including incoherence, wave-passage and differential site-response effects, *Earthquake Engineering & Structural Dynamics* 41 (3) (2012) 495–513. doi:10.1002/eqe.1141.
- [40] E. H. Field, T. E. Dawson, K. R. Felzer, A. D. Frankel, V. Gupta, T. H. Jordan, T. Parsons, M. D. Petersen, R. S. Stein, R. J. Weldon, C. J. Wills, Uniform California Earthquake Rupture Forecast, Version 2 (UCERF 2), *Bulletin of the Seismological Society of America* 99 (4) (2009) 2053 –2107. doi:10.1785/0120080049.
- [41] D. J. Wald, T. I. Allen, Topographic slope as a proxy for seismic site conditions and amplification, *Bulletin of the Seismological Society of America* 97 (5) (2007) 1379–1395. doi:10.1785/0120060267.
- [42] N. Basöz, J. Mander, Enhancement of the highway transportation lifeline module in HAZUS, Tech. rep., Final Pre-Publication Draft (#7) prepared for the National Institute of Building Sciences (NIBS) (1999).
- [43] K. Ramanathan, R. DesRoches, J. Padgett, Analytical fragility curves for multispan continuous steel girder bridges in moderate seismic zones, *Transportation Research Record: Journal of the Transportation Research Board* 2202 (-1) (2010) 173–182. doi:10.3141/2202-21.
- [44] R. Lee, A. S. Kiremidjian, Uncertainty and correlation for loss assessment of spatially distributed systems, *Earthquake Spectra* 23 (4) (2007)

- 560 753–770. doi:10.1193/1.2791001.
- 561 [45] J. W. Baker, Introducing correlation among fragility functions for multiple components, in: 14th World Conference on Earthquake Engineering, Beijing, China, 2008, p. 8.
- 562 [46] S. Werner, C. Taylor, S. Cho, J. Lavoie, REDARS 2 methodology and software for seismic risk analysis of highway systems (technical manual), Tech. rep., Seismic Systems & Engineering Analysis for MCEER, Oakland, CA (2006).
- 563 [47] Caltrans, Caltrans Seismic Design Criteria Version 1.7, Tech. Rep. SDC 1.7, California Department of Transportation, Sacramento, CA (2013).
- 564 [48] Bechtel/HNTB Team, Design Criteria Volume I, Version 1.2, Tech. rep., San Francisco Bay Area Rapid Transit District, San Francisco Bay Area Rapid Transit District Earthquake Safety Program (2008).
- 565 [49] K. N. Ramanathan, Next generation seismic fragility curves for California bridges incorporating the evolution in seismic design philosophy, PhD thesis, Georgia Institute of Technology (2012).
- 566 [50] N. Kurtz, J. Song, P. Gardoni, Time-varying seismic reliability analysis of representative US west coast bridge transportation networks, in: G. Deodatis, B. R. Ellingwood, D. M. Frangopol (Eds.), Safety, Reliability, Risk and Life-Cycle Performance of Structures and Infrastructures, CRC Press, 2014, pp. 655–662.
- 567 [51] J. Ghosh, K. Rokneddin, J. E. Padgett, L. DueasOsorio, Seismic reliability assessment of aging highway bridge networks with field instrumentation data and correlated failures. i: Methodology, Earthquake Spectra doi:10.1193/040512eqs155m.
- 568 [52] S. Pugh, Construction statistics, Tech. rep., California Department of Transportation Division of Engineering Services (2012).
- 569 [53] K. Kockelman, Travel Behavior as Function of Accessibility, Land Use Mixing, and Land Use Balance: Evidence from San Francisco Bay Area, *Transportation Research Record: Journal of the Transportation Research Board* 1607 (-1) (1997) 116–125. doi:10.3141/1607-16.
- 570 [54] E. A. Vasconcellos, Rural transport and access to education in developing countries: policy issues, *Journal of Transport Geography* 5 (2) (1997) 127–136. doi:10.1016/S0966-6923(96)00075-0.
- 571 [55] P. Waddell, F. Nourzad, Incorporating nonmotorized mode and neighborhood accessibility in an integrated land use and transportation model system, *Transportation Research Record: Journal of the Transportation Research Board* 1805 (-1) (2002) 119–127. doi:10.3141/1805-14.
- 572 [56] K. A. Small, *Urban Transportation Economics*, Psychology Press, 1992.
- 573 [57] C. F. Manski, *Structural analysis of discrete data with econometric applications*, MIT Press, 1981.
- 574 [58] K. A. Small, H. S. Rosen, Applied welfare economics with discrete choice models, *Econometrica* 49 (1) (1981) 105–130. doi:10.2307/1911129.
- 575 [59] D. Ory, Personal communication (2013).
- 576 [60] United States Department of Transportation, Revised departmental guidance: valuation of travel time in economic analysis, US Department of Transportation, Washington, DC.
- 577 [61] E. Stergiou, Treatment of uncertainties in seismic risk analysis of transportation systems, Engineer thesis, Stanford University (2006).
- 578 [62] N. Shiraki, M. Shinozuka, J. E. Moore, S. E. Chang, H. Kameda, S. Tanaka, System risk curves: Probabilistic performance scenarios for highway networks subject to earthquake damage, *Journal of Infrastructure Systems* 13 (1) (2007) 43–54. doi:10.1061/(ASCE)1076-0342(2007)13:1(43).
- 579 [63] G. Erhardt, P. Brinckerhoff, D. Ory, A. Sarvepalli, J. Freedman, J. Hood, B. Stabler, MTC's Travel Model One: applications of an activity-based model in its first year, in: *Innovations in Travel Modeling 2012*, Tampa, Florida, 2012, p. 9.
- 580 [64] P. Waddell, UrbanSim: modeling urban development for land use, transportation, and environmental planning, *Journal of the American Planning Association* 68 (3) (2002) 297–314. doi:10.1080/01944360208976274.
- 581 [65] W. Davidson, P. Vovsha, J. Freedman, R. Donnelly, CT-RAMP family of activity-based models, in: *Proceedings of the 33rd Australasian Transport Research Forum (ATRF)*, Canberra, Australia, 2010, p. 15.
- 582 [66] Citilabs, Cube desktop (2013).
- 583 [67] N. Basöz, A. Kiremidjian, Risk assessment for highway transportation systems, PhD thesis, Stanford University (1996).
- 584 [68] H. Wakabayashi, H. Kameda, Network performance of highway systems under earthquake effects: a case study of the 1989 Loma Prieta earthquake, in: *Proceedings US-Japan Workshop on Earthquake Disaster Prevention for Lifeline Systems*, 1992, pp. 215–232.
- 585 [69] A. A. Hagberg, D. A. Schult, P. J. Swart, Exploring network structure, dynamics, and function using NetworkX, in: *Proceedings of the 7th Python in Science Conference (SciPy2008)*, Pasadena, CA USA, 2008, p. 1115.
- 586 [70] D. Ory, R. Singh, Initial examination of volume delay functions using PeMS data, memorandum (2012).
- 587 [71] National Cooperative Highway Research Program (NCHRP), Predicting air quality effects of traffic-flow improvements: Final report and user's guide, NCHRP Report 535, Transportation Research Board, Washington D.C. (Jan. 2005).
- 588 [72] H.-W. Lim, J. Song, N. Kurtz, Seismic reliability assessment of lifeline networks using clustering-based multi-scale approach, in review (2014).
- 589 [73] P. Wang, T. Hunter, A. M. Bayen, K. Schechtner, M. C. Gónzalez, Understanding road usage patterns in urban areas, *Scientific Reports* 2. doi:10.1038/srep01001.
- 590 [74] C. Purvis, Data and analysis methods for metropolitan-level environmental justice assessment, *Transportation Research Record: Journal of the Transportation Research Board* 1756 (-1) (2001) 15–21. doi:10.3141/1756-02.
- 591 [75] A. Fothergill, E. G. M. Maestas, J. D. Darlington, Race, ethnicity and disasters in the United States: a review of the literature, *Disasters* 23 (2) (1999) 156–173. doi:10.1111/1467-7717.00111.
- 592 [76] U.S. Bureau of the Census, United states census 2010, Tech. rep., U.S. Census Bureau, Washington D.C. (2010).